

# Guide-star assisted imaging through multimode optical fibres

Shuhui Li,<sup>1,2,\*</sup> Simon A. R. Horsley,<sup>1</sup> Tomáš Tyc,<sup>3</sup> Tomáš Čížmár,<sup>4,5</sup> and David B. Phillips<sup>1,†</sup>

<sup>1</sup>Physics and Astronomy, University of Exeter, Exeter, EX4 4QL, UK.

<sup>2</sup>Wuhan National Laboratory for Optoelectronics, Huazhong University of Science and Technology, Wuhan 430074, Hubei, China.

<sup>3</sup>Department of Theoretical Physics and Astrophysics, Masaryk University, Kotlarska 2, 61137 Brno, Czech Republic.

<sup>4</sup>Leibniz Institute of Photonic Technology, Albert-Einstein-Straße 9, 07745 Jena, Germany.

<sup>5</sup>Institute of Scientific Instruments of CAS, Kr'álovopolská 147, 612 64, Brno, Czech Republic.

When light propagates through an opaque scattering material, the spatial information it holds becomes scrambled, but not necessarily lost. Two powerful classes of techniques have emerged in recent years to recover this information, enabling us to see *through* opaque media. Firstly, the scattering properties of a sample may be measured and subsequently cancelled out using transmission matrix (TM) based approaches. These methods describe the scattering as a linear matrix operator relating incident and transmitted fields. Secondly, optical memory effects reveal underlying correlations between incident and transmitted light, which can be exploited to image through opaque objects. Optical memory effects have been extensively studied in thin randomly scattering layers, which exhibit shift and tilt correlations that can be leveraged for imaging. In this work we develop a general framework describing the nature of optical memory effects in a broader class of structures of more arbitrary geometry. We show how this framework, when combined with wavefront shaping driven by feedback from a guide-star, enables estimation of an *approximate* transmission matrix (ATM) describing the scattering properties of any of these systems. This highlights that guide-star assisted imaging is possible regardless of the type of memory effect a scatterer exhibits. We study multimode optical fibres (MMFs) within our general framework, and identify a ‘quasi-radial’ memory effect. We experimentally demonstrate a new way to characterise and *partially* image through MMFs, only requiring access to their proximal end, with potential applications to flexible ultra-thin micro-endoscopes. These concepts broaden the applications of optical memory effects to a range of novel imaging and optical communication scenarios.

Coherent images are encoded in spatial light modes: patterns in the intensity and phase of light. When these patterns propagate through an opaque scattering material, such as frosted glass, a multimode optical fibre, or biological tissue, they distort and fragment, and the spatial information they carry becomes scrambled. This corrupts the formation of images of objects hidden behind or inside turbid media. In the last decade or so, a series of pioneering studies have demonstrated how digital light shaping technology can be used to measure and reverse scattering effects - unscrambling the light back to the state it was in before it entered the medium [1–4]. These techniques take advantage of the linear (in electric field) and deterministic nature of the scattering, and have enabled focussing and imaging through scattering systems [5–9]. At the heart of this capability lies the transmission matrix (TM) concept, which describes the scattering as a linear operation relating a set of input spatial light modes incident on one side of the scatterer, to a new set of output modes leaving on the opposite side [3]. Once the TM of a scatterer has been measured, it tells us what input field is required to create an arbitrary output field, and thus permits the transmission of images through the scatterer. However, measurement of the TM typically requires full optical access to both sides of the scatterer - impossible when the image plane is, for example, embedded in living tissue.

To overcome this limitation and look *inside* scattering en-

vironments, a useful suite of tools has emerged in the form of optical memory effects: the presence of underlying correlations between the incident and transmitted fields [10–13]. These hidden correlations have been extensively studied in thin randomly scattering layers which have direct applications to imaging through biological tissue. In this case tilting [10], shifting [12], spectral [14] and temporal [15] correlations have been revealed. The tilt and shift memory effects are related to correlations in the Fourier-space or real-space TM of a scatterer - and have enabled extraction of subsets of the TM which can be used to image over small areas inside scattering systems.

In parallel with these advances, TM approaches have also spurred the development of alternative methods of seeing into tissue much more deeply, albeit invasively, by guiding light along narrow waveguides. These techniques use multimode optical fibres (MMFs) to achieve high-resolution imaging at the tip of a needle - acting as ultra-low footprint endoscopes. Modal dispersion scrambles coherent optical signals transmitted through MMFs, and so before they can be deployed in scanning imaging systems, their TM must also first be measured. MMF based micro-endoscopy has great potential for deep tissue imaging, as indicated by a swathe of recent successes [16–19], yet a major challenge holding back broader uptake of this technique is the fragility of the TM used to control the optical field at the distal (far) facet. After TM calibration, which as described above conventionally requires access to both ends of the fibre, the MMF must be held completely static, as even small perturbations in fibre configuration (e.g. bends or twists) or temperature de-phase the propagating fibre modes, severely reducing the contrast of focussed spots at the

\*Electronic address: shli@hust.edu.cn

†Electronic address: d.phillips@exeter.ac.uk

distal facet, and the fidelity of the reconstructed images. *Flexible* operation of micro-endoscopic imaging systems based on current optical fibre technology require a TM characterisation method that can be rapidly performed on the fibre in-situ, with access only at the proximal (near) end.

Here we develop a general framework describing how monochromatic memory effects arise in samples of arbitrary geometry, and apply it to the MMF case. We show that deployment of a guide-star located on the distal facet of a MMF (and capable of reporting its local field intensity to the proximal end), combined with an estimate of the basis in which the TM is close to diagonal, provides a way to approximate the TM of, and thus image through, optical fibres. Crucially, this approach only requires access to the proximal end of the MMF: offering a route to *in-situ* TM calibration of flexible micro-endoscopic imaging systems. More generally, the concept we describe here enables guide-star based scanning imaging to be performed through scattering systems of any geometry, *without* invoking conventional shift or tilt memory effects, as long as we have an estimate of the basis in which the TM is quasi-diagonal. Our work broadens the applications of memory effects beyond thin randomly scattering layers to a range of novel imaging and optical communication scenarios.

### The memory effect in an arbitrary basis

We start by describing the emergence of memory effects in optical systems of arbitrary geometry. These systems may encompass, for example, the well-understood case of thin scattering layers, but also networks of wave-guides, or any other linear optical system through which light is transmitted. We assume that we know the geometry of the object before us - for example a thin scattering layer, or an optical fibre - but we do not have detailed knowledge of its scattering properties - for example we do not know the spatial function of the refractive index throughout a layer, or the length or bend configuration of a fibre. Given this level of prior information, we describe when and how optical memory effects may be used to achieve imaging.

In the general case, our aim is to image through a scattering system that has an unknown monochromatic TM,  $\mathbf{T}$ . As a first step, let's assume that the geometry of the system reveals enough information for us to estimate a basis in which  $\mathbf{T}$  is *approximately* diagonal, i.e.  $\mathbf{T} = \mathbf{U}\mathbf{D}\mathbf{U}^{-1}$ , where we know matrix  $\mathbf{U}^{-1}$  which allows us to transform to the quasi-diagonal basis from knowledge of the field in real-space. We assume that  $\mathbf{D}$  is quasi-diagonal (i.e. it has a significant proportion of its power concentrated on the diagonal), but we have no knowledge of the complex elements of  $\mathbf{D}$ . We consider the following questions: is advanced knowledge of a basis in which the TM of a scatterer is quasi-diagonal enough information to (i) predict a memory effect in, and (ii) image through, the system?

The memory effect occurs when a given modulation (i.e. transformation) of the field incident onto a scatterer modifies the output field in a deterministic way - for example, creat-

ing a lateral displacement of the output field. To explore this idea in a general basis, we express the input field as a column vector  $\mathbf{u}$ , which holds the complex coefficients of the input field in real-space. Incident field  $\mathbf{u}$  is transformed into an output field  $\mathbf{v} = \mathbf{T}\mathbf{u}$  via propagation through a scatterer. We consider a modulation of the incident field in the form  $\mathbf{u}' = \mathbf{O}\mathbf{u} = \mathbf{U}\mathbf{M}\mathbf{U}^{-1}\mathbf{u}$ , where  $\mathbf{M}$  is a diagonal matrix. After such a modulation, the output field  $\mathbf{v}$  is changed to  $\mathbf{v}'$ , which can be written as

$$\mathbf{v}' = \mathbf{T}\mathbf{u}' = \mathbf{U}\mathbf{D}\mathbf{M}\mathbf{U}^{-1}\mathbf{u}. \quad (1)$$

Given that  $\mathbf{M}$  is exactly diagonal, and  $\mathbf{D}$  is close to diagonal, the two matrices will commute with an error  $[\mathbf{D}, \mathbf{M}]$  that is due to the off-diagonal elements of  $\mathbf{D}$ , i.e.  $\mathbf{D}\mathbf{M} = \mathbf{M}\mathbf{D} + [\mathbf{D}, \mathbf{M}]$ . As  $\mathbf{D}$  becomes closer to diagonal this error will reduce, becoming zero in the limit of an exactly diagonal matrix. We therefore rewrite Eq. (1) as

$$\begin{aligned} \mathbf{v}' &= \mathbf{U}\mathbf{M}\mathbf{D}\mathbf{U}^{-1}\mathbf{u} + \mathbf{U}(\mathbf{D}\mathbf{M} - \mathbf{M}\mathbf{D})\mathbf{U}^{-1}\mathbf{u} \\ &= \mathbf{O}\mathbf{T}\mathbf{u} + \mathbf{U}[\mathbf{D}, \mathbf{M}]\mathbf{U}^{-1}\mathbf{u}, \end{aligned} \quad (2)$$

which shows that for input transformations of the form  $\mathbf{O} = \mathbf{U}\mathbf{M}\mathbf{U}^{-1}$ , the output field undergoes the same transformation with an error  $\boldsymbol{\eta} = \mathbf{U}[\mathbf{D}, \mathbf{M}]\mathbf{U}^{-1}\mathbf{u}$ . In more condensed notation, Eq. (2) is

$$\mathbf{v}' = \mathbf{O}\mathbf{v} + \boldsymbol{\eta} \sim \mathbf{O}\mathbf{v}. \quad (3)$$

Equation (3) describes a general form of the memory effect. In answer to our first question (i), Eqn. (3) tells us that without knowing anything about the elements of the quasi-diagonal matrix  $\mathbf{D}$ , we can deterministically modify the field transmitted through a scattering system. The basis in which the TM is diagonal is linked to the form of the field modification, i.e. memory effect, that is possible. This highlights the existence of an infinite family of memory effects operating in scattering systems of different geometries, each requiring its own unique but predictable set of transformations on input fields, with a deterministic transformation of the output that is not, in general, a translation of the field. We now focus on some special cases, and highlight when imaging is possible using these memory effects.

### Memory effect based imaging through scattering systems

First consider the well-known tilt-tilt memory effect [10, 11]. In a thin randomly scattering layer, multiple scattering is governed at a statistical level by a diffusion process, meaning that light focussed to a given lateral position on the input will only diffuse locally to nearby lateral positions at the output. In this case our assumption is that  $\mathbf{U} = \mathbf{I}$ , the identity matrix, i.e. the monochromatic TM is quasi-diagonal in the position basis (and equivalently exhibits diagonal correlations in the Fourier basis [12]). Our transformation  $\mathbf{O}$  is thus also diagonal in the position basis:  $\mathbf{O} = \mathbf{I}\mathbf{M}\mathbf{I} = \mathbf{M}$ . This means that any spatially varying phase change applied to the input field, is also applied to the output field. More specifically, a tilt of the input

beam results in a tilt of the output beam, in which case the diagonal elements of  $\mathbf{M}$  correspond to a phase ramp modulation given by  $\mathbf{M} = \text{diag}[e^{i(\delta k_x \mathbf{x} + \delta k_y \mathbf{y})}]$ , where  $\text{diag}[\mathbf{d}]$  places vector  $\mathbf{d}$  on the main diagonal of a square zero matrix,  $\mathbf{x}$  and  $\mathbf{y}$  are vectors specifying the  $x$  and  $y$  coordinates of each pixel on the input plane, and  $\delta k_x$  and  $\delta k_y$  specify the desired change in  $x$ - and  $y$ -components of the wave-vector normal to the tilted wavefront.

Tilting of the output beam is not in itself useful to image the output plane of the sample. However, in the far-field of the output, this tilt corresponds to a lateral shift, and so unknown speckle patterns can be controllably translated in the far-field. Bertolotti et al. [20] showed that imaging is then possible from the input side by measuring the fluorescent intensity excited by these unknown patterns as they are scanned in two dimensions. This procedure yields the amplitudes of the Fourier components of the image, but not the phases of these Fourier components. Despite this missing information, a diffraction limited image of an object in the far-field can be estimated using a phase retrieval algorithm with appropriate constraints [21].

Next consider the more recently discovered shift–shift memory effect [12]. This occurs for some anisotropic disordered materials, assuming that the scatterer has a thickness less than the transport mean-free-path (TMFP) of the system. The TMFP is the average length over which scattering randomises the photon direction (wave-vector). This means that we expect only small changes in the angular deviation of rays from input to output, and so assume the TM of the scatterer to be quasi-diagonal when represented in the two dimensional Fourier basis  $\mathbf{U} = \mathcal{F}^{-1}$ . In this case a transformation  $\mathbf{O} = \mathcal{F}^{-1}\mathbf{M}\mathcal{F}$  of the input beam leads to approximately the same transformation of the output beam. Again choosing a phase ramp along the diagonal of  $\mathbf{M}$ ,  $\mathbf{O}$  becomes a spatial shift operator, and so lateral displacement of the input beam results in a corresponding shift of the output beam, i.e.  $\mathbf{M} = \text{diag}[e^{-i(\mathbf{k}_x \delta x + \mathbf{k}_y \delta y)}]$ , where  $\mathbf{k}_x$  and  $\mathbf{k}_y$  are vectors specifying the  $x$ - and  $y$ -components of the wave-vectors arriving at the input plane, and  $\delta x$  and  $\delta y$  specify the desired lateral shift of the input. Equivalently the TM exhibits diagonal correlations in real-space [12]. In this case, imaging in the near-field of the output is possible by scanning unknown speckle patterns in 2D and performing phase retrieval [20].

The addition of a ‘guide-star’ embedded in the scatterer provides more information, and so improves the memory effect based imaging that is possible: yielding images with higher signal-to-noise, and without the need for phase-retrieval. First implemented in astronomy to correct for atmospheric turbulence [22], a guide-star is a point within the scatterer capable of signalling the intensity of its local field to the outside world. For use in microscopy, guide-stars have been created from highly reflective embedded particles [23], or via a range of alternative methods exploiting, for example,

fluorescent [24], magnetic [25], movement-based [26], photo-acoustic [27], or acousto-optic [28] properties. The input field required to focus on a guide-star,  $\mathbf{u}^{\text{gs}}$ , can be calculated by phase conjugation of a field emanating from the guide-star [2], or by phase stepping holography [4].  $\mathbf{u}^{\text{gs}}$  constitutes a single column of the inverse of the TM of the scatterer,  $\mathbf{T}^{-1}$  (with the output discretised in the real-space ‘pixel’ basis). In cases where the TM is unitary (or at least approximately so),  $\mathbf{T}^{-1} = \mathbf{T}^\dagger$ , and knowledge of  $\mathbf{u}^{\text{gs}}$  is equivalent to knowing one row of the TM [29].

Memory effects that laterally shift the output field (such as the tilt and shift memory effects described above) can be understood to arise from the existence of correlations in the real-space TM of the scatterer (or its Fourier transform), so that measuring one row of the TM also provides information about other rows [12]. Therefore once  $\mathbf{u}^{\text{gs}}$  is found, these shift memory effects can be exploited to controllably scan the focus over a local area around the guide-star, known as the isoplanatic patch. The size of the isoplanatic patch is governed by the distance over which the output field can be translated before it de-correlates (i.e. the degree to which the approximation in Eqn. (3) holds). This strategy has been used to create scanning imaging systems inside randomly scattering samples by a suitable combination of tilting and/or lateral translation of the input wavefront [30, 31]. Therefore, in an initial answer to our second question (ii), so far it has been shown that diffraction limited imaging is possible using the shift–shift and tilt–tilt memory effects, which are capable of laterally translating the output field in two dimensions.

### Rotational and radial memory effects in multimode fibres

We now consider the emergence of memory effects in other geometries, and examine a MMF as a key example. The near cylindrical symmetry of MMFs leads to the prediction of a basis in which the TM is approximately diagonal. For example, solving the wave equation in an idealised straight section of step index fibre at a single wavelength results in a set of orthogonal circularly polarised eigenmodes that maintain a constant spatial profile and polarisation on propagation [32]. Here, following work by Plöeschner et al. [33], we refer to these modes as propagation invariant modes (PIMs). Even though real optical fibres differ from this idealised case, it was recently shown in ref. [33] that the TM of a short length of step index MMF is relatively diagonal when represented in the PIM basis.

Following our general framework, in this case  $\mathbf{U} = \mathbf{P}$ , the matrix transforming from the PIM basis to real-space, and so the TM of a MMF can be factorised according to  $\mathbf{T} = \mathbf{P}\mathbf{D}\mathbf{P}^\dagger$ , where as before  $\mathbf{D}$  is quasi-diagonal, and here we have used the conjugate transpose  $\mathbf{P}^\dagger$  in place of the inverse  $\mathbf{P}^{-1}$  under the assumption that  $\mathbf{P}$  is sufficiently over-sampled in real-space such that  $\mathbf{P}\mathbf{P}^\dagger \propto \mathbf{I}$ . Figure (1a) shows a low-dimensional example of these matrices for a MMF that supports 42 modes per polarisation at a wavelength of 633 nm. Circularly polarised PIMs are specified by an azimuthal and radial index,  $\ell$  and  $p$  respectively. For a step index fibre of

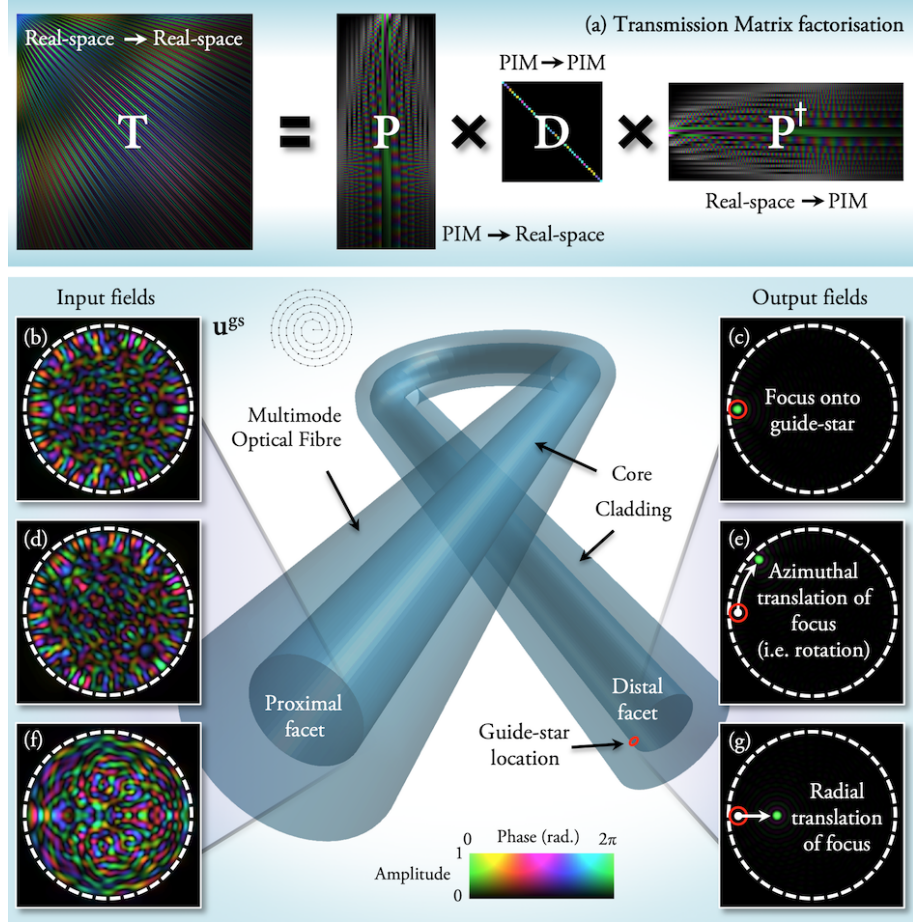


FIG. 1: **Field transformations through multimode fibres:** (a) The TM of an ideal MMF may be factorised into the product of three matrices. Shown is a low-dimensional example of these matrices for an ideal MMF that supports 42 modes per polarisation at a wavelength of 633 nm. Colour indicates phase, and brightness indicates amplitude of the complex elements (as shown in scale bar in lower panel). When real-space pixels are ordered outwards along an Archimedes spiral (example shown inset), translational correlations in the real-space TM are highlighted, i.e. a single row is similar to a spatially shifted copy of adjacent rows. (b) shows an example of a proximal field  $\mathbf{u}^{\text{gs}}$  required to form a focus (shown in green in (c)) onto a guide-star at the edge of the distal facet of an ideal fibre (position of guide-star indicated by a red circle). Due to the rotational memory effect, by rotating the input field around the fibre axis (d) the output field is rotated by the same angle, moving the focus azimuthally (e). Using knowledge of  $\mathbf{u}^{\text{gs}}$  and  $\mathbf{P}$  enables estimation of the TM of the system, and prediction of the proximal field (f) required to radially translate the focus (g). These simulations model an ideal fibre supporting 754 modes per polarisation at a wavelength of 633 nm - this mode capacity is used for simulations throughout the rest of the paper.

radius  $a$ , the transverse field of  $\psi_{\ell,p}$ , in cylindrical coordinates (denoted by radial position  $r$  and azimuthal position  $\theta$ ), is given by

$$\psi_{\ell,p}(r, \theta) = N_{\ell,p} e^{i\ell\theta} \begin{cases} \mathcal{J}_{\ell}(u_{\ell,p}r/a) / \mathcal{J}_{\ell}(u_{\ell,p}) & \text{for } r < a \\ \mathcal{K}_{\ell}(\omega_{\ell,p}r/a) / \mathcal{K}_{\ell}(\omega_{\ell,p}) & \text{for } r \geq a, \end{cases} \quad (4)$$

where  $N_{\ell,p}$  is a normalisation constant ensuring all modes have a total intensity equal to 1,  $\mathcal{J}_{\ell}$  is a Bessel function of the first kind of order  $\ell$ , and  $\mathcal{K}_{\ell}$  is a modified Bessel function of the second kind of order  $\ell$ .  $u_{\ell,p}$  and  $\omega_{\ell,p}$  are normalised transverse wave-numbers of each PIM in the core and cladding respectively, which may be found from the roots of the characteristic equation describing the parameters of the fibre (see ref. [32] and Methods for more details).  $\ell$ , the vortex charge, is proportional to the amount of orbital angular momentum

(OAM) carried by the PIM, which is characterised by a helical wavefront that accrues a phase change of  $2\pi\ell$  around one circuit of the fibre axis [34].

Equation (3) leads to an input modulation of  $\mathbf{O} = \mathbf{PMP}^{\dagger}$ , which tells us that phase changes imparted to individual PIMs at the input of the fibre are preserved at the output. Applying a phase ramp modulation linearly proportional to azimuthal mode index  $\ell$ , i.e.  $\mathbf{M} = \text{diag}[e^{-i\ell\delta\phi}]$ , is equivalent to rotating the input field around the fibre axis by an angle  $\delta\phi$ . Here  $\ell$  is a vector specifying the vortex charge of each PIM. As these  $\ell$ -dependent phase changes are preserved at the output, the output field is also rotated by  $\delta\phi$ . This effect is already well-known, and coined the rotational memory effect [35]. Our general framework tells us that it is a rotational analogue of the shift-shift memory effect: the angular dependence of

the MMF TM is quasi-diagonal in the 1D cylindrical Fourier basis (i.e. the OAM basis), and therefore an angular shift of the input field leads to an angular shift of the output field. Figure (1a) shows the corresponding diagonal correlations in the real-space TM, when the real-space pixels are ordered along, for example, an Archimedes spiral, winding out from the central axis of the fibre (see inset in Fig. (1)).

We might wonder whether there is a corresponding effect where we can displace the output field from the fibre in a radial direction. Equation (3) shows that the form of memory effect based field transformation is intrinsically linked to the basis in which the TM is diagonal. As shown in all three cases above, a displacement operation is diagonalized in the Fourier basis. Therefore, without knowledge of the TM, any *lateral displacement* of the unknown output field is only possible in systems where the TM is quasi-diagonal in the Fourier basis. The radial dependence of the MMF TM is not quasi-diagonal in the Fourier basis. This means that a ‘radially-shifting’ memory effect, that serves to translate the entire output field of a MMF radially, does not occur - and in any case, such translations would be ill-defined at the fibre axis and core-cladding interface. In the Supplementary Information (SI) Section §S1, we explore the disruption of shifting memory effects in MMFs in more detail. We show how the presence of the fibre edges - the core-cladding interface - breaks the translational symmetry thus disrupting the equivalent of the 2D shift-shift memory effect in MMFs.

Despite this, modulations that operate on the field in the radial direction do exist. For example, consider the effect of a modulation based on the radial mode index  $p$  on the input beam:  $\mathbf{M} = \text{diag}[e^{i p \delta \rho}]$ , i.e. a phase ramp linearly proportional to  $p$ , where vector  $\mathbf{p}$  holds the radial index of each PIM, and where  $\delta \rho = \pi \delta r / a$ , and  $\delta r$  is radial distance across the fibre facet. Such a modulation may be viewed as a ‘quasi-radial’ memory effect: although as described above, it can’t enable a simple translation of the distal field.

Figure 2 shows the behaviour of the quasi-radial memory effect. Intriguingly, if the output field is concentrated to a diffraction limited spot centred on the fibre axis, then the above modulation on the input field does indeed correspond to a radial shift of this point - i.e. it is transformed into a ring of intensity of radius  $\delta r$  (see Fig. (2a)). However, output fields corresponding to diffraction limited points at other radii on the distal facet show a variety of different transformations, depending on the radial coordinate of the point (see Figs. (2b-d)). We emphasise that all of these transforms are independent of the length of the fibre. This tells us that if the field is localised to a diffraction limited spot anywhere on the distal facet, the intensity pattern can be deterministically transformed - with a fidelity governed once again by how well the approximation in Eqn. (3) holds.

In SI §S2 we explore two other quasi-radial memory effects: Firstly we show that if the position of the initial focussed spot is known, then this information enables a phase-only modulation linearly proportional to the radial

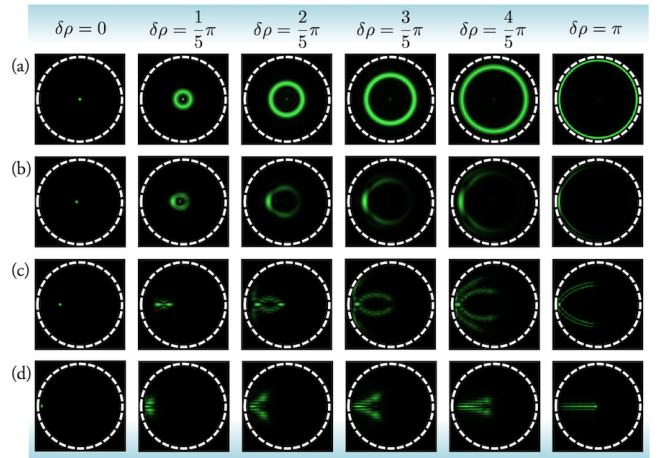


FIG. 2: **The quasi-radial memory effect in MMFs:** Each row shows simulations of a sequence of distal intensity patterns obtained by applying an input modulation  $\mathbf{O} = \mathbf{PMP}^{-1}$  using  $\mathbf{M} = \text{diag}[e^{i p \delta \rho}]$ , for increasing  $\delta \rho$ , where the initial distal field (left most panel) is a diffraction limited spot at four different radial coordinates: on the fibre axis (a), just off fibre axis (b), midway between fibre axis and core-cladding boundary (c), and near core-cladding boundary (d). We see a variety of different predominantly radial transformations take place. All of these are independent of the length of the fibre (i.e. independent of elements of  $\mathbf{D}$ ). We note that if the initial spot position is rotated about the fibre axis, so are these output fields, by virtue of the rotational memory effect.

component of the wave-vectors composing the modes,  $k_r$ , to be applied - which is capable of moving the spot with less distortion than shown in Fig. 2 (although still not perfectly). Secondly we show that a modulation of the form  $\mathbf{M} = \text{diag}[\cos(\mathbf{u}_{\ell,p} r / a)]$  enables a point to be radially expanded about its initial position, wherever that may be on the distal facet. Yet for an arbitrary speckled output beam, these radially varying transformations all interfere in a way that cannot be predicted without knowledge of the amplitudes and phases of the original distal speckle field - which itself requires knowledge of the entire TM.

### Guide-star assisted imaging through MMFs

The lack of a true ‘radially shifting’ memory effect has implications for imaging through uncalibrated MMFs. As scanning of *unknown* speckle patterns is only permitted in 1D (azimuthally), then there is no way to perform imaging based on 2D scanning of these speckle patterns as in ref [20]. However, provided we know how to focus the field at the output to a point, the existence of the quasi-radial memory effects suggests a form of ghost imaging might be possible. For example, a sequence of known intensity patterns could be projected to the distal end of the fibre using the rotational and quasi-radial memory effects, and their level of overlap with the distal scene recorded back at the proximal end by measuring the total intensity of the return signal, allowing an image to be computationally reconstructed [36, 37]. Although this idea holds promise, we now show that it is possible to do even

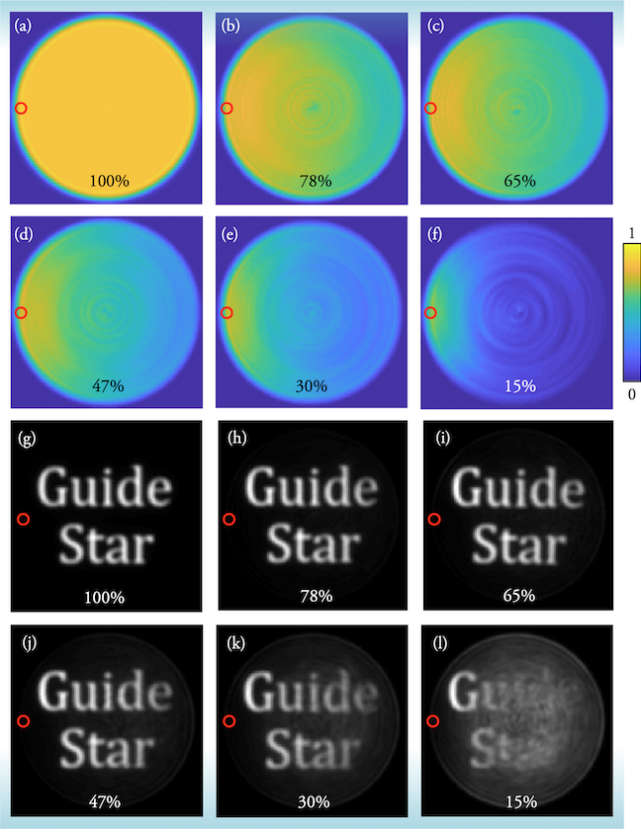


FIG. 3: **The size and shape of the isoplanatic patch:** (a-f) Simulated maps of the power-ratio of points focussed to different regions of the distal facet through non-ideal fibres with quasi-diagonal TM  $\mathbf{D}$ . Foci are created using ATM  $\mathbf{D}'$  calculated from  $\mathbf{u}^{\text{gs}}$  using Eqn. (7).  $p_a$ , the power on the diagonal of  $\mathbf{D}$ , decreases from panel (a) to (f) and is given at bottom of each panel. (g-l) Simulations of scanning imaging capabilities in each case. We see that the isoplanatic patch gradually shrinks around the location of the guide-star (red circles).

better, and use the information held in matrix  $\mathbf{P}$  (i.e. knowledge of the basis in which the TM is quasi-diagonal), to scan a well-defined focus around a guide-star in both azimuthal and *radial* directions. This opens up a 2D isoplanatic patch at the output of the fibre, within which scanning imaging is possible.

We imagine placing a single guide-star, such as a fluorescent particle, at the distal facet of the fibre (see the red circle on the fibre schematic in Fig. (1)). The proximal field that will focus onto the guide-star,  $\mathbf{u}^{\text{gs}}$ , can be measured using phase stepping holography, with access only to the proximal end, as described in, for example, ref. [4], or in a single shot using phase conjugation [2].

So far, guided by Eqn. (3), we have restricted ourselves to transforms on the input field of a particular form  $\mathbf{O} = \mathbf{U}\mathbf{M}\mathbf{U}^{-1}$ . We now relax this and consider more general transformations of the input field to achieve a radial shift in the position of a focused spot on the distal facet. To accomplish output field modulations beyond what is possible with conventional memory effects alone (such as in this case), knowledge

of the full TM of the scatterer is required - see SI §S1 for more discussion. Fortunately, it is indeed possible to obtain an estimate of the TM using the information at our disposal. In the case of a MMF, we can make the assumption that the TM is unitary (i.e. power loss is minimal). We also assume the TM to be *perfectly* diagonal in the PIM basis. Under these assumptions, we can now find  $\mathbf{D}'$ , a diagonal approximation to the true quasi-diagonal TM  $\mathbf{D}$ . To proceed, we show that the measurements on the guide-star reveal the phase delay of each PIM due to propagation through the MMF. This phase information can then be used to populate the complex elements along the main diagonal of  $\mathbf{D}'$ , while setting all off-diagonal elements to zero.

More specifically, the defining equation for the input field  $\mathbf{u}^{\text{gs}}$  that focuses onto a guide-star is

$$\mathbf{T}\mathbf{u}^{\text{gs}} = \mathbf{P}\mathbf{D}'\mathbf{u}^{\text{gs}} = \mathbf{v}^{m_0}, \quad (5)$$

where we denote the output field focused onto the guide-star as  $\mathbf{v}^{m_0}$ , which has all elements equal to zero except for one at the spatial point corresponding to the location of the guide-star, indexed by  $m_0$ . Substituting the perfectly diagonal approximation  $\mathbf{D}'$  that we wish to find in place of the real quasi-diagonal TM  $\mathbf{D}$ , and multiplying both sides of Eqn. (5) by the adjoint of  $\mathbf{P}$  then gives  $\mathbf{D}'\mathbf{P}^\dagger\mathbf{u}^{\text{gs}} = \mathbf{P}^\dagger\mathbf{v}^{m_0}$ . Our assumption of unitarity means that the elements of the diagonal matrix  $\mathbf{D}'$  only vary by their phase term, so the  $n^{\text{th}}$  element  $D'_{nn} = \exp(i\phi_n)$ . Therefore we can also re-write the defining equation for  $\mathbf{u}^{\text{gs}}$  as

$$e^{i\phi_n} \sum_m P_{nm}^\dagger u_m^{\text{gs}} = P_{n,m_0}^\dagger. \quad (6)$$

If we can estimate the PIM basis  $\mathbf{P}$  and we know the input field  $\mathbf{u}^{\text{gs}}$  that focuses onto the guide-star at  $m_0$ , we can estimate the phases on the diagonal of  $\mathbf{D}'$  by rearranging Eqn. (6) for  $e^{i\phi_n}$ , yielding

$$D'_{nn} = e^{i\phi_n} = e^{i(\sigma_n - \gamma_n)}, \quad (7)$$

where the two contributions to the phase are given by

$$\sigma_n = \arg [P_{nm_0}^\dagger], \quad (8)$$

$$\gamma_n = \arg \left[ \sum_m P_{nm}^\dagger u_m^{\text{gs}} \right]. \quad (9)$$

Here  $\gamma_n$  is the phase delay mode  $n$  picks up on propagation through the fibre, and  $\sigma_n$  is a mode dependent phase correction term, equal to the relative phase required for each PIM to constructively interfere at the lateral location of the guide-star if it were positioned at the *proximal* end of the MMF. The intuition behind  $\sigma_n$  is to ensure that we incorporate only the phase delay due to the scatterer into the estimated TM, and remove any apparent phase delay associated purely due to the choice of diagonal basis. The *Approximate Transmission Matrix* (ATM) of the MMF in the real-space basis is then given by  $\mathbf{T}' = \mathbf{P}\mathbf{D}'\mathbf{P}^\dagger$ . The ATM can now be used to predict the

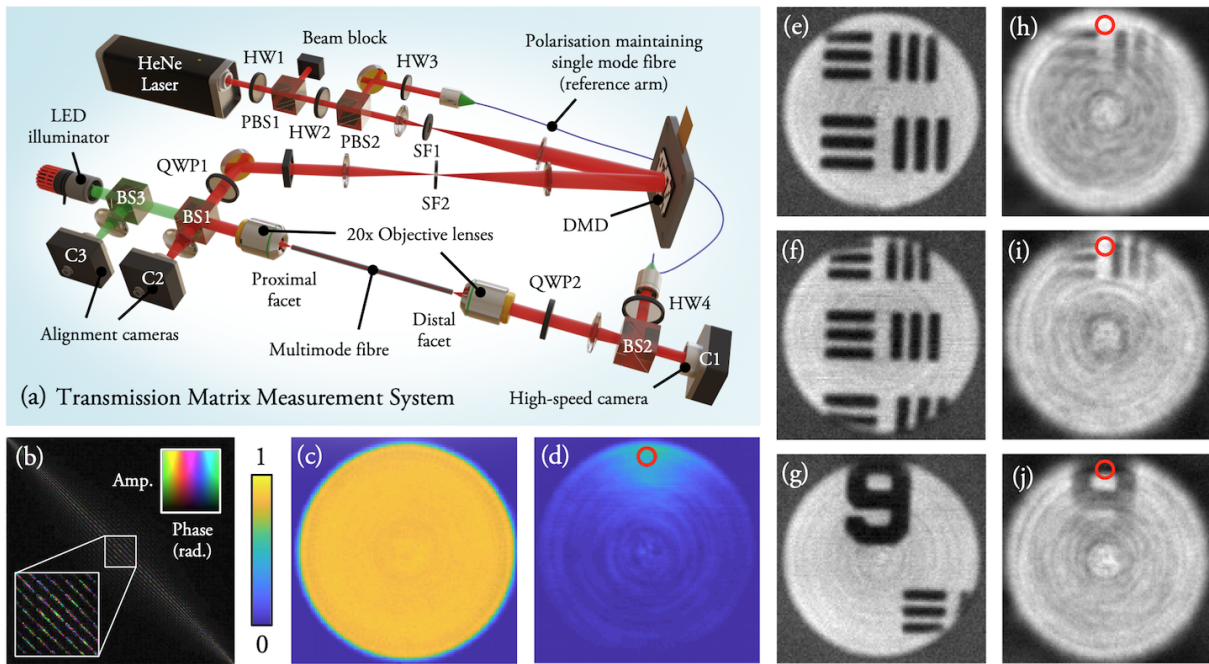


FIG. 4: **Proof of principle experiments:** (a) Experimental set-up to measure the full TM of a MMF, emulate ATM measurement with a guide-star, and image through the MMF using the full TM and ATM. HW = half wave-plate, QW = quarter wave-plate, BS = beamsplitter, PBS = polarizing beamsplitter, SF = spatial filter. SI §S3 provides a more detailed description of the set-up. (b) Fully sampled TM of MMF represented in PIM basis. Inset shows an enlarged region of the TM indicating the fine structure around the main diagonal. A larger version of this figure is shown in SI (§S4). (c,d) Power ratio maps of scanned foci using the fully sampled TM (c) and guide-star based ATM (d). Guide-star location is marked with a red circle. (e-g) Example transmission images of a resolution target obtained with the fully sampled TM. (h-j) Examples of transmission images of the same scene as (e-g), in this case obtained with guide-star based ATM.

proximal field modulations required to move the focus both azimuthally and radially. Evidently, as will be shown later, knowledge of the ATM gives more general control over the output field than simply shifting the position of a focus.

The fidelity of the ATM will clearly depend upon how well we can estimate the basis in which the TM is diagonal (i.e. the validity of the approximation in Eqn. (3)). Figure (3) shows simulations of the imaging performance through a MMF as our ability to accurately estimate the diagonal basis is compromised. We simulate the measurement of  $\mathbf{u}^{\text{gs}}$  using a guide-star placed at the core-cladding boundary (marked by a red circle in Fig. (3)), and construct the ATM. See Methods for a detailed description of these simulations, which capture how power is spread away from the diagonal of the TM in a realistic manner. Figures (3a-f) show the power-ratio (i.e. the ratio of power focussed into a target spot using the ATM compared to total power transmitted to the distal facet), as  $p_d$ , the percentage of power on the main diagonal of the real TM  $\mathbf{D}$ , decreases. Each panel maps how the power-ratio varies over the distal facet - capturing the size and shape of the isoplanatic patch. We see that the error in the ATM is non-uniformly distributed over its columns - meaning that columns representing points close to the guide-star are well captured, while the errors in columns representing points further away grow with distance from the guide-star. This results in an isoplanatic patch that gradually

collapses around the location of the guide-star as  $p_d$  reduces. Figures (3g-l) show simulations of the guide-star based imaging performance, indicative of the spatial variation in contrast and resolution in each case. Here imaging across the entire facet appears to be disrupted once  $p_d$  falls below  $\sim 25\%$ .

### Proof of principle experiments

In order to test our concept in practice, we design an experiment capable of measuring the full TM of a step index MMF (NA = 0.22, core diameter =  $50 \mu\text{m}$ ,  $\sim 30 \text{ cm}$  in length) supporting 754 spatial modes per polarisation at a wavelength of 633 nm. These dimensions are chosen as a typical example of a MMF that may find micro-endoscopic imaging applications. The experimental set-up is similar to that described in ref. [38] and is shown in Fig. (4(a)). The spatial mode of input light is controlled using a digital micro-mirror device (DMD) in the Fourier plane of the proximal fibre facet, and the distal fibre facet is imaged onto a high-speed camera, along with a coherent reference beam enabling extraction of the complex field via phase stepping holography (See Methods and SI §S3 and §S4 for more details).

We first fully sample the TM of the MMF. After correcting for coarse misalignments in the input and output beams following the strategy outlined in ref. [33], and transforming to the PIM basis representation, the fully sampled TM possesses  $p_d \sim 15\%$  of its power on the main diagonal (TM shown in

Fig. (4b)). Therefore in this experiment we anticipate a guide-star assisted imaging performance equivalent to that predicted in Fig. (3f) - i.e. an isoplanatic patch extending around the guide-star, but not reaching across the entire output facet of the fibre.

Figures (4c,d) show the experimentally measured power ratio maps of foci generated at the distal facet of the fibre using the fully sampled TM (4c), and a guide-star based ATM (4d). The ATM was constructed from data recorded by a single pixel of the camera imaging the output facet, mimicking the action of a guide-star. The extent of the isoplanatic patch in Fig. (4d) matches well with Fig. (3f) as predicted. Figures (4e-g) show transmission images of a resolution target using the fully sampled TM. Figures (4h-j) show the same scenes imaged using the ATM (more detail of how these images was recorded is given in Methods). As expected, we see that imaging is possible through a small isoplanatic patch around the guide-star, and objects outside this patch are not discernible as we are unable to create a high contrast focus in these regions. This gradual reduction in resolution and contrast away from the guide-star is analogous to the situation found in memory effect based imaging through thin scattering layers.

We note that in these experiments, the object (resolution target) is positioned  $\sim 40 \mu\text{m}$  away from the distal facet of the fibre. Therefore, in order to reconstruct an image of the object in focus, the scanned foci had to be axially refocussed from the distal facet to the object plane. Due to the cylindrical symmetry of the fibre, the radial k-vector ( $k_r = \sqrt{k_x^2 + k_y^2}$ ) of input light is approximately preserved at the output - which is a consequence of the quasi-diagonal nature of the fibre TM in the PIM basis. Therefore, as previously demonstrated in refs. [17, 39], refocussing is achieved by adding a quadratic ‘lensing’ phase term directly to the field that is generated by the DMD. This means that we actually create fields corresponding to defocussed spots at the distal facet of the fibre, which then focus onto the resolution target. Despite this increase in complexity, Figs. (4h-j) demonstrate that this can be successfully achieved using the ATM, which affords a high level of control over the field within the isoplanatic patch. SI §S5 shows the refocussing capability in more detail.

In addition to imaging, it is also possible to project patterns through the MMF into the isoplanatic patch, examples of which are shown in SI §S6. We also studied the effect of fibre deformation on guide-star assisted focusing, and found only a minor reduction in the power-ratio of foci was observed when the fibre was bent through  $90^\circ$  with a radius of curvature of  $\sim 10 \text{ cm}$ , as shown in SI §S7. This result shows there is potential for applying single-ended guide-star based TM calibration to image through flexible MMFs undergoing time varying deformations.

The location of the guide-star on the distal facet also plays a key role in determining the accuracy of the ATM, and thus the size and shape of the isoplanatic patch. We can only measure the phase change of PIMs that have an intensity

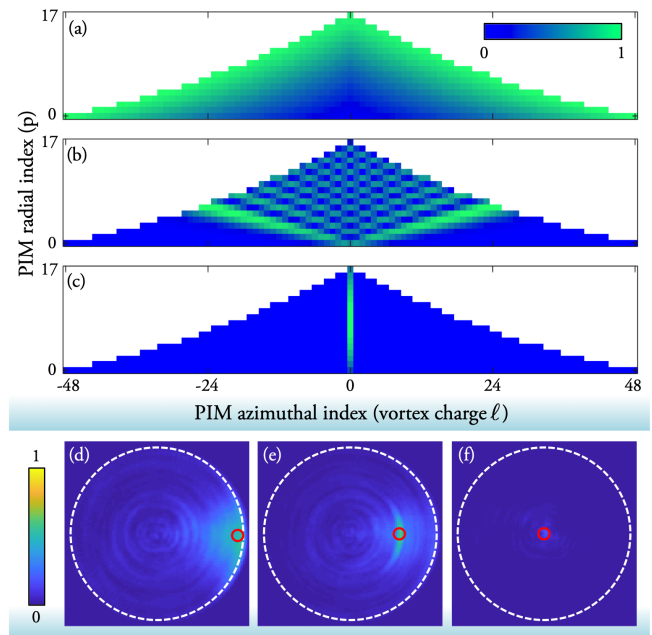


FIG. 5: **Choice of guide-star location:** (a-c) Theoretical absolute values of the level of overlap of all PIMs with three different guide-star locations. Maps (a,b,c) corresponds to guide-star locations shown by red circles in (d,e,f). The colour of point  $\ell, p$  in PIM maps represents the relative level of overlap of  $\psi_{\ell,p}$  with the specified guide-star location. (d-f) Experimentally measured power ratio maps using ATMs reconstructed from guide-stars in the three different locations, marked with red circles. A guide-star positioned at the core-cladding interface gives the greatest level of overlap with all of the PIMs and therefore the largest isoplanatic patch. A guide-star positioned on the fibre axis achieves the lowest level of overlap with the PIMs, and the isoplanatic patch shrinks to a single diffraction limited point in this case.

profile that overlaps with the guide-star position. Therefore, it is preferable to choose a guide-star location that overlaps with the highest number of PIMs. Inspecting the rows of matrix  $\mathbf{P}$ , which hold this overlap information, reveal that guide-star locations at the core-cladding boundary overlap with all of the PIMs - although we note that some PIMs of index  $\ell = 0$  will have very low intensity at the edge of the core as their fields are concentrated mainly on the fibre axis. It is straight forward to test this in our experiment - moving the guide-star simply means choosing a different camera pixel to use for ATM construction. Figure (5) shows the experimental power ratio maps for three different choices of guide-star location, along with plots showing the theoretical level of overlap with the PIMs in each case. As expected, the area of the isoplanatic patch is maximised when the guide-star is placed on the core-cladding boundary.

## Discussion

There is one point on the distal facet that we know how to focus on perfectly: the position of the guide-star itself, which has been directly measured. However, as can be seen in both simulations and experiments (Figs. (3) and (4)), as  $p_d$  de-

creases, then using the ATM does not yield a perfect focus even onto the guide-star itself. This is a consequence of our assumptions that the fibre TM is perfectly diagonal and unitary - assumptions that become less accurate with lower values of  $p_d$ . To mitigate this, when scanning over the guide-star location, the proximal field returned by the ATM can be replaced with  $\mathbf{u}^{\text{gs}}$ . Points at the same radius as the guide-star may also be created with a higher power ratio than achievable with the ATM, by rotating the field used to generate the guide-star focus around the fibre axis - i.e. directly employing the rotational memory effect [35]. This observation also points to a more sophisticated approach to reconstruct the ATM: instead of forcing  $\mathbf{D}'$  to be diagonal, we could try to iteratively search for a  $\mathbf{D}'$  allowing the minimum power in off-diagonal elements, so that it also perfectly focussed onto the guide-star. This is a severely under-constrained problem that we plan to investigate in more detail in the future.

Equation 7 stipulates that we must know the location of the guide-star on the distal facet, in order to apply the phase correction term  $\sigma$ . However, if the location of the guide-star is unknown and  $\sigma$  is omitted (i.e.  $\sigma = 0$ ),  $\mathbf{D}'$  still provides an estimate of the TM of the MMF, but with an unknown rotation between the proximal and distal planes. We note that in this case, the radial location of a guide-star at an unknown position can be retrieved, as it is uniquely encoded in the relative amplitudes of the PIMs overlapping with the guide-star, which extracted by decomposing  $\mathbf{u}^{\text{gs}}$  in the PIM basis. This implies that the methods presented here may be possible even without specifically engineering a guide-star on the distal facet of the fibre. For example, a guide-star may be formed at a random location by optimising a non-linear feedback signal at the proximal end of the fibre [40]. Once the proximal field required to generate a focus,  $\mathbf{u}^{\text{gs}}$ , is found, the focus can then be scanned in 2D using the methods we have presented here.

We highlight that recently there have been several innovative proposals to achieve single ended TM characterisation of a MMF. For example, Gu et al. proposed recovery of the forward TM by measurement of the round trip reflection matrix of a fibre in which the distal facet has been engineered with a partial reflector of spatially varying reflection coefficient, and moveable shutter [41]. The same group more recently suggested a simpler approach with a uniform partial reflector that can go some way to improving spot formation [42]. Gordon et al. proposed the placement of a stack of patterned spectral filters at the distal facet and recovering the forward TM by measuring the reflection matrix at multiple frequencies [43]. Chen et al. proposed placing a compact spatial multiplexer at the distal facet capable of imprinting a mode dependent time delay or frequency modulation [44]. The engineering requirements of these proposals are technically challenging, and so they have yet to be experimentally realised in MMFs of high enough resolution to be useful for imaging. The re-imaging properties of graded index fibres have also been demonstrated to enable a spot to be focussed at a chosen location within up to half of a distal facet using a non-linear feedback signal from two-photon fluorescence [45]. However, in this case,

an optimisation process taking on the order of several minutes was required to achieve a focus at each new location. The guide-star assisted imaging concept we present here is arguably simpler than these recent proposals, although it may be more limited in terms of the accuracy of the forward TM that can be recovered, and the length of the fibre that may be calibrated. Ultimately, we hope that some combination of our concept and the alternative strategies above may provide the most robust solution to this important problem.

In summary, we have demonstrated the possibility of guide-star assisted imaging through multimode fibres, which can be calibrated with access only to the proximal end of the fibre. We believe this technique to hold promise for the development of flexible multimode fibre based imaging systems. The reconstruction of the ATM, and of the images through the fibre, requires no iterative phase retrieval, and invokes no assumptions about the statistical properties of the scene at the end of the fibre - instead relying on assumptions about the properties of the fibre itself. Using a high speed DMD capable of modulating input light at  $\sim 20$  kHz, measurement of the proximal field that focuses on a fluorescent guide-star,  $\mathbf{u}^{\text{gs}}$  (from which the ATM is calculated) consisting of, for example,  $\sim 1000$  modes can be performed in  $\sim 200$  ms using phase stepping holography [38, 46]. Using a highly reflective guide-star, the same calibration could potentially be achieved in a single shot - albeit with lower SNR [2, 23] (SI §S8 contrasts these two methods). Therefore both calibration and imaging can be performed in real-time.

In our proof of principle experiments, the isoplanatic patch does not extend over the full area of the distal facet. However our simulations show (see Fig. (3)) that the area of this isoplanatic patch can be significantly increased by making a better estimate of the basis in which the TM of the MMF is diagonal. Such an estimate can be achieved by optimising the fibre parameters with access to the full TM, before subsequent deployment of the system as a flexible micro-endoscope [33], which will be a focus of our efforts in future work. To image through longer MMFs which possess higher levels of mode coupling (and therefore lower values of  $p_d$  even after fibre parameter optimisation), we envisage that multiple guide-stars, distinguished by, for example, emission frequency or speckle pattern contrast [47], could be used to increase the total area of the distal facet through which it is possible to image.

Beyond applications to optical fibres, and in answer to our questions posed earlier, we have shown that guide-star assisted imaging need not invoke tilt or shift memory effects, and can be extended to any scattering system in which we have an estimate of the basis in which the TM is quasi-diagonal. Prior knowledge of this sort can be understood as a generalisation of the concept of the transport mean free path to spaces other than the momentum basis, i.e. advanced knowledge that a scattering system possesses an optical path length that is much lower than a 'generalised' transport mean free path in a known (arbitrary) basis. The diagonal nature of the TM indicates that spatial modes input in the diagonal basis are not randomised into the entire vector space describing the

allowed modes within the structure. Other optical systems to which this concept may be applied, in addition to step-index MMFs as we have demonstrated in this work, include graded index [48] and photonic crystal fibres [49], few-mode fibre bundles (which have the constraint that the guide-star is ideally placed in the far-field of the output [50]), photonic lanterns [51], opaque walls (i.e. imaging around corners) [52], and artificially engineered photonic networks and scattering systems.

## METHODS

### Construction of matrix $\mathbf{P}$

To perform guide-star assisted imaging through MMFs, we must estimate matrix  $\mathbf{P}$ , that transforms from the propagation invariant mode (PIM) basis to real-space. The PIMs are found by solving the wave equation in a cylindrical geometry. This reduces to finding the roots of the scalar characteristic equations describing the modal dispersion [32].

$$u \frac{J_{\ell-1}(u)}{J_{\ell}(u)} + \omega \frac{K_{\ell-1}(\omega)}{K_{\ell}(\omega)} = 0, \quad (10)$$

where  $J_{\ell}$  is a Bessel function of the first kind of order  $\ell$ , and  $K_{\ell}$  is a modified Bessel function of the second kind of order  $\ell$ .  $u$  and  $\omega$  are normalised transverse wave-numbers which are related to the fibre parameters through

$$u = a (k^2 n_{\text{core}}^2 - \beta^2)^{\frac{1}{2}}, \quad (11)$$

$$\omega = a (\beta^2 - k^2 n_{\text{core}}^2)^{\frac{1}{2}}, \quad (12)$$

$$\omega^2 = v^2 - u^2, \quad (13)$$

$$v = ak\text{NA}, \quad (14)$$

$$\text{NA}^2 = n_{\text{core}}^2 - n_{\text{clad}}^2. \quad (15)$$

Here  $a$  is the radius of the core, NA is the numerical aperture of the fibre and  $n_{\text{core}}$  and  $n_{\text{clad}}$  are the refractive indices of the core and cladding respectively.  $k$  is the vacuum wavenumber:  $k = 2\pi/\lambda$ , where  $\lambda$  is the vacuum wavelength.  $\beta$  is the propagation constant describing the phase velocity of each mode. Eqn. 10 may have multiple roots  $u_{\ell,p}$ , indexed by the vortex charge  $\ell$  specified in the order of the Bessel functions, and radial index  $p$  which counts the roots for a particular choice of  $\ell$ . Once the roots have been found, the function  $\psi_{\ell,p}(r, \theta)$  represents the complex 2D field profile of the mode indexed by  $\ell, p$  according to Eqn. 4.  $\omega_{\ell,p}$  are related to  $u_{\ell,p}$  through Eqn. 13, and  $r$  and  $\theta$  are the radial and azimuthal coordinates respectively across the core. Roots with a real phase velocity  $\beta_{\ell,p}$  are propagating modes within the core.  $K_{\ell}$  takes argument  $\omega_{\ell,p}$ , which is imaginary when  $\beta_{\ell,p} < k^2 n_{\text{core}}^2$ . This then describes the evanescent field in the cladding of the fibre (i.e. for the region  $r \geq a$ ). The PIMs, indexed by  $\ell, p$  are ordered into a 1D list, indexed by  $n$ . Once the 2D complex functions describing each PIM have been

found, column  $n$  of matrix  $\mathbf{P}$  is constructed by representing the complex field of the  $n^{\text{th}}$  PIM in Cartesian coordinates on a 2D grid, and reshaping it into a column vector.

### Simulations

The optical transformation properties of fibres in real-space are modelled following the methods in ref. [33], by decomposing real space input fields into the PIMs, multiplying by a TM represented in the PIM $\leftrightarrow$ PIM basis ( $\mathbf{D}$ ), and transforming back to real space (see Fig. (1a)):  $\mathbf{T} = \mathbf{PDP}^{\dagger}$ .

An ideal fibre (as simulated in Figs. (1) and (2)), of length  $L$  is modelled by a diagonal matrix  $\mathbf{D}$ , where the  $n^{\text{th}}$  diagonal element is given by  $e^{iL\beta_n}$ . To model non-ideal fibres with quasi-diagonal TMs in the PIM basis, as shown in Fig. (3), misalignment matrices  $\mathbf{R}$  are introduced that transform the real-space field at each end of the fibre into a new real-space basis that is laterally ( $dx$  and  $dy$ ) and axially ( $dz$ ) shifted, and tilted (about  $x$  and  $y$ ), and defocussed a small randomly chosen amount. A quasi-diagonal  $\mathbf{D}_q$  with realistic off-diagonal coupling is created by absorbing these misalignment matrices into the TM in the PIM $\leftrightarrow$ PIM basis, i.e.  $\mathbf{D}_q = \mathbf{R}_{\text{dl}}^{\dagger} \mathbf{D} \mathbf{R}_{\text{pr}}$ , where  $\mathbf{R}_{\text{pr}}^{\dagger} = \mathbf{P}^{\dagger} \mathbf{R}_{\text{pr}} \mathbf{P}$  and  $\mathbf{R}_{\text{dl}}^{\dagger} = \mathbf{P}^{\dagger} \mathbf{R}_{\text{dl}} \mathbf{P}$  are the two different misalignment operators at the proximal and distal end of the fibre respectively here represented in the PIM basis. Therefore to reduce the power on the diagonal ( $p_d$ ) of  $\mathbf{D}_q$ , and spread it off the diagonal in a realistic manner, the magnitudes of the randomly chosen misalignment in each dimension are increased.

Figure (3) shows modelling of the reconstruction of the ATM, and the performance of using it to focus and image through the fibre  $p_d$  is decreased. To simulate this, we use  $\mathbf{T} = \mathbf{PD}_q \mathbf{P}^{\dagger}$  to calculate the field required to focus on the guide-star,  $\mathbf{u}^{\text{gs}}$ , where  $\mathbf{u}^{\text{gs}} = \mathbf{T}^{\dagger} \mathbf{v}^{m_0}$ , and column vector  $\mathbf{v}^{m_0}$  represents the desired field in vectorised form (i.e. zeros everywhere except for 1 at the element  $m_0$  corresponding to the location of the guide-star).  $\mathbf{u}^{\text{gs}}$  is then used to reconstruct the ATM  $\mathbf{T}'$  according to Eqns. (7-9). The ATM  $\mathbf{T}'$  is then used to calculate the estimated input fields required to raster scan a focus across the distal facet of the fibre, which are then propagated through the real TM  $\mathbf{T}$ , enabling the power ratio maps and reconstructed images to be modelled.

### Binary amplitude hologram design

A DMD is used to shape the light into the MMF during TM measurement and for imaging. To generate an arbitrary (bandwidth limited) spatially varying complex field  $\mathcal{A} = A(x, y) e^{i\alpha(x, y)}$  in the first diffraction order in the Fourier plane of the DMD ( $x$  and  $y$  being Cartesian coordinates of real-space in the optical Fourier plane of the DMD), we encode the inverse Fourier transform of  $\mathcal{A}$ , i.e.  $\mathcal{B} = \mathcal{F}^{-1}(\mathcal{A}) = B(x', y') e^{i\gamma(x', y')}$ , into a binary amplitude hologram to be displayed on the DMD,  $\mathbf{H}(x', y')$ . Here  $x'$  and  $y'$  are Cartesian coordinates on the DMD chip. Following [53, 54],

$\mathbf{H}(x', y')$  is given by:

$$\mathbf{H}(x', y') = \frac{1}{2} + \frac{1}{2} \operatorname{sgn} [\cos(p(x', y')) - \cos(q(x', y'))], \quad (16)$$

where

$$p(x', y') = \gamma(x', y') + \phi_{\text{tilt}}(x', y'), \quad (17)$$

$$q(x', y') = \arcsin \left[ \frac{B(x', y')}{B_{\text{max}}} \right], \quad (18)$$

and where  $B_{\text{max}}$  is the maximum amplitude of  $B$ , and  $\phi_{\text{tilt}}(x', y') = k_x x' + k_y y'$  is a phase gradient directing the desired beam into the first diffraction order at an angle defined by wave-vectors  $k_x$  and  $k_y$ . This hologram  $\mathbf{H}$  can be intuitively understood as one in which the local phase of the grating (i.e. local lateral position of the grating cycle) varies in proportion with the desired phase of the target complex field, and the local duty cycle of the grating varies as a function of the desired amplitude.  $\mathbf{H}$  also results in light transmitted into other diffraction orders, which can be spatially filtered in the Fourier plane of the DMD, leaving only the desired optical field transmitted into the rest of the optical system. The wave-vectors  $k_x$  and  $k_y$  also place a bandwidth limit on the complex field that can be generated and still successfully separated from other diffraction orders in the Fourier plane of the DMD.

### Imaging through guide-star calibrated MMFs

The experimental setup, along with TM and ATM measurement are described in detail in SI §S3 and §S4. Once the TM and ATM are measured, they are used to capture the scanning imaging results are presented in Fig. (4). A transmissive resolution target mounted on a manually operated 3D translation stage was manoeuvred to  $\sim 40 \mu\text{m}$  from the distal facet of the fibre. The scanning spot was refocused from the distal fibre facet to the plane of the resolution target by adding a quadratic Fresnel lens phase function to the hologram displayed on the DMD. The fully sampled TM or the ATM was used to calculate the proximal fields required to attempt to raster scan the focus across the resolution target. At each spot position  $x, y$ , the total transmitted intensity arriving at camera C1 was recorded ( $I(x, y)$ ), which directly represented pixel  $x, y$  of the reconstructed image. We also attempted reflection based imaging by using a reflective resolution target and recording the total intensity of light reflected back through the fibre to camera C3. However we found that reflection images were very noisy due to the low laser power (1 mW) of the laser available for the experiment. Reflection imaging through MMFs has been successfully demonstrated in the past, but due to the low numerical aperture of MMFs, signals are typically very low when imaging beyond the end of the fibre facet, as we were doing here, and so laser powers on the order of at least several hundred mW are necessary for the return signal to be accurately measured. Reflection imaging using the ATM should be possible in future work using higher power lasers.

- [1] Ivo M Vellekoop and AP Mosk. Focusing coherent light through opaque strongly scattering media. *Optics letters*, 32(16):2309–2311, 2007.
- [2] Zahid Yaqoob, Demetri Psaltis, Michael S Feld, and Changhuei Yang. Optical phase conjugation for turbidity suppression in biological samples. *Nature photonics*, 2(2):110, 2008.
- [3] SM Popoff, G Lerosey, R Carminati, M Fink, AC Boccarda, and S Gigan. Measuring the transmission matrix in optics: an approach to the study and control of light propagation in disordered media. *Physical review letters*, 104(10):100601, 2010.
- [4] Tomáš Čižmár, Michael Mazilu, and Kishan Dholakia. In situ wavefront correction and its application to micromanipulation. *Nature Photonics*, 4(6):388, 2010.
- [5] Ivo M Vellekoop, Aart Lagendijk, and AP Mosk. Exploiting disorder for perfect focusing. *Nature photonics*, 4(5):320, 2010.
- [6] Sébastien Popoff, Geoffroy Lerosey, Mathias Fink, Albert Claude Boccarda, and Sylvain Gigan. Image transmission through an opaque material. *Nature communications*, 1:81, 2010.
- [7] Roberto Di Leonardo and Silvio Bianchi. Hologram transmission through multi-mode optical fibers. *Optics express*, 19(1):247–254, 2011.
- [8] Allard P Mosk, Ad Lagendijk, Geoffroy Lerosey, and Mathias Fink. Controlling waves in space and time for imaging and focusing in complex media. *Nature photonics*, 6(5):283, 2012.
- [9] Stefan Rotter and Sylvain Gigan. Light fields in complex media: Mesoscopic scattering meets wave control. *Reviews of Modern Physics*, 89(1):015005, 2017.
- [10] Shechao Feng, Charles Kane, Patrick A Lee, and A Douglas Stone. Correlations and fluctuations of coherent wave transmission through disordered media. *Physical review letters*, 61(7):834, 1988.
- [11] Isaac Freund, Michael Rosenbluh, and Shechao Feng. Memory effects in propagation of optical waves through disordered media. *Physical review letters*, 61(20):2328, 1988.
- [12] Benjamin Judkewitz, Roarke Horstmeyer, Ivo M. Vellekoop, Ioannis N. Papadopoulos, and Changhuei Yang. Translation correlations in anisotropically scattering media. *Nature Physics*, 11:684 EP –, 06 2015.
- [13] Hasan Yilmaz, Chia Wei Hsu, Arthur Goetschy, Stefan Bittner, Stefan Rotter, Alexey Yamilov, and Hui Cao. Angular memory effect of transmission eigenchannels. *Physical Review Letters*, 123(20):203901, 2019.
- [14] Johannes F de Boer, Meint P van Albada, and Ad Lagendijk. Transmission and intensity correlations in wave propagation through random media. *Physical Review B*, 45(2):658, 1992.
- [15] Mykola Kadobianskyi, Ioannis N Papadopoulos, Thomas Chaigne, Roarke Horstmeyer, and Benjamin Judkewitz. Scattering correlations of time-gated light. *Optica*, 5(4):389–394, 2018.
- [16] Youngwoon Choi, Changhyeong Yoon, Moonseok Kim, Tae-seok Daniel Yang, Christopher Fang-Yen, Ramachandra R Dasari, Kyoung Jin Lee, and Wonshik Choi. Scanner-free and wide-field endoscopic imaging by using a single multimode optical fiber. *Physical review letters*, 109(20):203901, 2012.
- [17] Tomáš Čižmár and Kishan Dholakia. Exploiting multimode waveguides for pure fibre-based imaging. *Nature communications*, 3:1027, 2012.
- [18] Shay Ohayon, Antonio Caravaca-Aguirre, Rafael Piestun, and James J DiCarlo. Minimally invasive multimode optical fiber microendoscope for deep brain fluorescence imaging. *Biomed-*

- ical optics express*, 9(4):1492–1509, 2018.
- [19] Sergey Turtaev, Ivo T Leite, Tristan Altwegg-Boussac, Janelle MP Pakan, Nathalie L Rochefort, and Tomáš Čižmár. High-fidelity multimode fibre-based endoscopy for deep brain in vivo imaging. *Light: Science & Applications*, 7(1):92, 2018.
- [20] Jacopo Bertolotti, Elbert G Van Putten, Christian Blum, Ad Lagendijk, Willem L Vos, and Allard P Mosk. Non-invasive imaging through opaque scattering layers. *Nature*, 491(7423):232, 2012.
- [21] James R Fienup. Reconstruction of an object from the modulus of its fourier transform. *Optics letters*, 3(1):27–29, 1978.
- [22] Robert Q Fugate, David L Fried, Guillermo A Ameer, BR Boeke, SL Browne, Paul H Roberts, RE Ruane, Glenn A Tyler, and LM Wopat. Measurement of atmospheric wavefront distortion using scattered light from a laser guide-star. *Nature*, 353(6340):144–146, 1991.
- [23] Seokchan Yoon, Moonseok Kim, Mooseok Jang, Youngwoon Choi, Wonjun Choi, Sungsam Kang, and Wonshik Choi. Deep optical imaging within complex scattering media. *Nature Reviews Physics*, pages 1–18, 2020.
- [24] Ivo M Vellekoop, Meng Cui, and Changhuei Yang. Digital optical phase conjugation of fluorescence in turbid tissue. *Applied physics letters*, 101(8):081108, 2012.
- [25] Haowen Ruan, Tom Haber, Yan Liu, Joshua Brake, Jinho Kim, Jacob M Berlin, and Changhuei Yang. Focusing light inside scattering media with magnetic-particle-guided wavefront shaping. *Optica*, 4(11):1337–1343, 2017.
- [26] Edward Haojiang Zhou, Haowen Ruan, Changhuei Yang, and Benjamin Judkewitz. Focusing on moving targets through scattering samples. *Optica*, 1(4):227–232, Oct 2014.
- [27] Fanting Kong, Ronald H Silverman, Liping Liu, Parag V Chitnis, Kotik K Lee, and Ying-Chih Chen. Photoacoustic-guided convergence of light through optically diffusive media. *Optics letters*, 36(11):2053–2055, 2011.
- [28] Benjamin Judkewitz, Ying Min Wang, Roarke Horstmeyer, Alexandre Mathy, and Changhuei Yang. Speckle-scale focusing in the diffusive regime with time reversal of variance-encoded light (trove). *Nature photonics*, 7(4):300, 2013.
- [29] Roarke Horstmeyer, Haowen Ruan, and Changhuei Yang. Guidestar-assisted wavefront-shaping methods for focusing light into biological tissue. *Nature photonics*, 9(9):563, 2015.
- [30] Gerwin Osnabrugge, Roarke Horstmeyer, Ioannis N. Papadopoulos, Benjamin Judkewitz, and Ivo M. Vellekoop. Generalized optical memory effect. *Optica*, 4(8):886–892, Aug 2017.
- [31] Ioannis N. Papadopoulos, Jean-Sébastien Jouhannau, James F. A. Poulet, and Benjamin Judkewitz. Scattering compensation by focus scanning holographic aberration probing (f-sharp). *Nature Photonics*, 11:116 EP –, 12 2016.
- [32] Katsunari Okamoto. *Fundamentals of optical waveguides*. Academic press, 2006.
- [33] Martin Plöschner, Tomáš Tyc, and Tomáš Čižmár. Seeing through chaos in multimode fibres. *Nature Photonics*, 9(8):529, 2015.
- [34] Jonathan Leach, Miles J Padgett, Stephen M Barnett, Sonja Franke-Arnold, and Johannes Courtial. Measuring the orbital angular momentum of a single photon. *Physical review letters*, 88(25):257901, 2002.
- [35] Lyubov V Amitonova, Allard P Mosk, and Pepijn WH Pinkse. Rotational memory effect of a multimode fiber. *Optics express*, 23(16):20569–20575, 2015.
- [36] Jeffrey H Shapiro. Computational ghost imaging. *Physical Review A*, 78(6):061802, 2008.
- [37] Lyubov V Amitonova and Johannes F De Boer. Compressive imaging through a multimode fiber. *Optics letters*, 43(21):5427–5430, 2018.
- [38] Sergey Turtaev, Ivo T Leite, Kevin J Mitchell, Miles J Padgett, David B Phillips, and Tomáš Čižmár. Comparison of nematic liquid-crystal and dmd based spatial light modulation in complex photonics. *Optics express*, 25(24):29874–29884, 2017.
- [39] Ivo T Leite, Sergey Turtaev, Xin Jiang, Martin Šiler, Alfred Cuschieri, Philip St J Russell, and Tomáš Čižmár. Three-dimensional holographic optical manipulation through a high-numerical-aperture soft-glass multimode fibre. *Nature Photonics*, 12(1):33–39, 2018.
- [40] Siddharth Sivankutty, Esben Ravn Andresen, Rosa Cossart, Géraud Bouwmans, Serge Monneret, and Hervé Rigneault. Ultra-thin rigid endoscope: two-photon imaging through a graded-index multi-mode fiber. *Optics express*, 24(2):825–841, 2016.
- [41] Ruo Yu Gu, Reza Nasiri Mahalati, and Joseph M Kahn. Design of flexible multi-mode fiber endoscope. *Optics express*, 23(21):26905–26918, 2015.
- [42] Ruo Yu Gu, Elaine Chou, Cory Rewcastle, Ofer Levi, and Joseph M Kahn. Improved spot formation for flexible multimode fiber endoscope using partial reflector. *arXiv preprint arXiv:1805.07553*, 2018.
- [43] George SD Gordon, Milana Gataric, Alberto Gil CP Ramos, Ralf Mouthaan, Calum Williams, Jonghee Yoon, Timothy D Wilkinson, and Sarah E Bohndiek. Characterizing optical fiber transmission matrices using metasurface reflector stacks for lensless imaging without distal access. *Physical Review X*, 9(4):041050, 2019.
- [44] Haoshuo Chen, Nicolas K Fontaine, Peter Winzer, Roland Ryf, and David Neilson. Single-end optical fiber transfer matrix measurement using spatial pilot, July 9 2019. US Patent 10,345,192.
- [45] Shamir Rosen, Doron Gilboa, Ori Katz, and Yaron Silberberg. Focusing and scanning through flexible multimode fibers without access to the distal end. *arXiv preprint arXiv:1506.08586*, 2015.
- [46] Donald B Conkey, Antonio M Caravaca-Aguirre, and Rafael Piestun. High-speed scattering medium characterization with application to focusing light through turbid media. *Optics express*, 20(2):1733–1740, 2012.
- [47] Antoine Boniface, Baptiste Blochet, Jonathan Dong, and Sylvain Gigan. Noninvasive light focusing in scattering media using speckle variance optimization. *Optica*, 6(11):1381–1385, 2019.
- [48] Joel Carpenter, Benjamin J Eggleton, and Jochen Schröder. 110x110 optical mode transfer matrix inversion. *Optics express*, 22(1):96–101, 2014.
- [49] Attila Mekis, JC Chen, I Kurland, Shanhui Fan, Pierre R Villeneuve, and JD Joannopoulos. High transmission through sharp bends in photonic crystal waveguides. *Physical Review Letters*, 77(18):3787, 1996.
- [50] Robert Kuschmierz, Elias Scharf, Nektarios Koukourakis, and Jürgen W Czarske. Self-calibration of lensless holographic endoscope using programmable guide stars. *Optics letters*, 43(12):2997–3000, 2018.
- [51] Debaditya Choudhury, Duncan K McNicholl, Audrey Repetttl, Itandehui Gris-Sánchez, Tim A Birks, Yves Wiaux, and Robert R Thomson. Compressive optical imaging with a photonic lantern. *arXiv preprint arXiv:1903.01288*, 2019.
- [52] Ori Katz, Pierre Heidmann, Mathias Fink, and Sylvain Gigan. Non-invasive single-shot imaging through scattering layers and around corners via speckle correlations. *Nature photonics*, 8(10):784, 2014.

- [53] Bryon R Brown and Adolf W Lohmann. Complex spatial filtering with binary masks. *Applied optics*, 5(6):967–969, 1966.
- [54] Wai-Hon Lee. Binary computer-generated holograms. *Applied Optics*, 18(21):3661–3669, 1979.

#### ACKNOWLEDGEMENTS

DBP thanks Dr Ben Sherlock for help with early parts of the experiment, Prof. Jacopo Bertolotti for useful discussions and careful reading of the manuscript, and Emily Beth Wai-See for encouragement. DBP and SL thank Dr Sergey Turtaev and Dr Ivo Leite for advice on setting up the experiment. SL acknowledges support from the National Natural Science Foundation of China under Grant no. 61705073. SARH acknowledges financial support from a Royal Society TATA University Research Fellowship (RPG-2016-186). TC thanks the European Regional Development Fund (CZ.

02.1.01/0.0/0.0/15\_003/0000476) and the European Research Council (724530) for financial support. DBP acknowledges financial support from the Royal Academy of Engineering and the European Research Council (804626).

#### AUTHOR CONTRIBUTIONS

DBP, TT and TC conceived the idea for the project. DBP supervised the project. SARH formulated the general memory effect theory. SARH, TT and DBP investigated the quasi-radial memory effect. DBP, SARH, TT and SL performed the simulations. SL built the optical setup and performed all experiments and analysis, with support from DBP and TC. DBP and SARH wrote the manuscript with editorial input from all other authors.